

Contents list available at CBIORE journal website

## Remarkable Energy Development

Journal homepage: https://ijred.cbiore.id



Research Article

## Synthesis of sodalite-natural dolomite as novel bifunctional catalyst for biodiesel production: Experimental study of performance and emissions on diesel engine

Misbakhul Fatah<sup>a</sup>, Abdul Hamid<sup>a</sup> , Zeni Rahmawati<sup>b</sup> , Saiful<sup>c</sup>, Tri Esti Purbaningtias<sup>d</sup> , Amin Jakfar<sup>a</sup>

**Abstract**. The development of catalysts derived from natural minerals was investigated in this study for biodiesel production due to their high catalytic activity, abundant availability, low production cost, and environmentally friendly. Biodiesel was produced from *Calophyllum Inophyllum* (CI) oil using bifunctional catalyst synthesized from natural dolomite and sodalite. In addition, an experimental study was conducted to evaluate the performance and emission characteristics of the produced biodiesel in a diesel engine. The natural dolomite catalyst contains a high composition of CaO-MgO, while sodalite, consisting of Si and Al precursors, was synthesized from natural kaolin. The bifunctional catalysts were synthesized via wet impregnation method with varying loadings of natural dolomite (5, 10, 15, 20, and 25 wt%). FTIR, XRD, SEM-EDX, and N2 adsorption-desorption analyses were employed to characterize the physicochemical properties of the catalysts. The optimum biodiesel yield of 94.14 % was obtained at dolomite loading of 25 wt%. Engine performance tests revealed that the B10 fuel blend produced maximum power and torque of 1.252 kW and 69.151 N.m., respectively, at 1250 rpm. While the optimum specific fuel consumption was obtained at 0.0004 Kg.HP/h at 1250 rpm for all fuel blends. The lowest CO emission was recorded for the B40 fuel blend at 414 ppm, while the lowest NO and NO<sub>x</sub> emissions were observed for the D100 fuel at 88 and 86 ppm, respectively.

Keywords: Biodiesel, Bifunctional Catalyst, Natural Dolomite, Sodalite, Diesel Engine



@ The author(s). Published by CBIORE. This is an open access article under the CC BY-SA license (http://creativecommons.org/licenses/by-sa/4.0/).

Received: 2<sup>nd</sup> June 2025; Revised: 18<sup>th</sup> July 2026; Accepted: 5<sup>th</sup> August 2025; Available online: 18<sup>th</sup> August 2025

### 1. Introduction

The global demand for energy continues to increase in line with economic growth and industrial development. However, the limitations and negative impacts associated with fossil fuel usage have raised several long-term sustainability concerns, particularly regarding environmental degradation (Brahma et al., 2022; Novita et al., 2024). In response, extensive research on renewable energy sources, including biodiesel production, has grown significantly. Biodiesel represents a sustainable alternative to conventional fossil fuels (Azhar et al., 2024; Darwin et al., 2023; Buchori et al, 2024). Moreover, biodiesel is a renewable biofuel produced from organic feedstocks such as waste cooking oil, agricultural residues, and animal fats, presenting a promising alternative owing to its biodegradable nature, environmental compatibility, and potential to mitigate greenhouse gas emissions (de S. Barros et al., 2020; Fiala et al., 2024; Kalita et al., 2022; Talebi et al., 2024).

Numerous studies have explored biodiesel production from edible oil feedstocks (Afsharizadeh & Mohsennia, 2021; Gamboa *et al.*, 2024; Mora *et al.*, 2024), however, this approach may compromise global food security by competing with food supply chains. Consequently, greater attention should be directed toward the development of biodiesel from non-edible

oil sources, which typically possess a high triglyceride content and offer a more sustainable alternative (Abdul Hakim Shaah *et al.*, 2021). *Calophyllum inophyllum* (CI) oil, commonly known as nyamplung oil, has emerged as a promising non-edible feedstock for sustainable biodiesel production (Aparamarta *et al.*, 2019). This plant is widely distributed across Indonesia, particularly in Bangkalan and Sampang, Madura Island. The seeds of CI contain a high crude oil content, ranging from 40 to 73%. Additionally, the oil contains approximately 70% triglycerides, making it a highly suitable biodiesel feedstock (Aparamarta *et al.*, 2022; Azhar *et al.*, 2024). Its fatty acid composition is dominated by oleic, linoleic, stearic, and palmitic acids (Fauzan *et al.*, 2020).

One challenge in biodiesel production lies in the high energy consumption of the transesterification process and the use of homogeneous catalysts, which cannot be reused under stoichiometric conditions. This has led to increased interest in heterogeneous catalysts, especially for industrial-scale applications (Widayat et al, 2024). Recently, a wide range of heterogeneous catalysts has been investigated for their potential in biodiesel production, including metal-based catalysts such as titanium(Emeji & Patel, 2024), (Hazmi et al., 2025), and zinc oxide (Hussain et al., 2022), as well as

Department of Mechanical and Industrial Engineering, Politeknik Negeri Madura, Sampang, 69281, Indonesia

<sup>&</sup>lt;sup>b</sup>Department of Chemistry, Faculty of Science and Data Analytics, Institut Teknologi Sepuluh Nopember, Surabaya 60111, Indonesia

<sup>&</sup>lt;sup>c</sup>Department of Mechanical Engineering, Universitas Muhammadiyah Surabaya, 60113, Indonesia

<sup>&</sup>lt;sup>d</sup>Department of Chemistry, Faculty of Mathematics and Natural Sciences, Universitas Islam Indonesia, Yogyakarta, 55584, Indonesia

<sup>\*</sup> Corresponding author Email: ahamchimie@poltera.ac.id (A. Hamid)

aluminosilicate-based catalysts such as zeolites (Saad *et al.*, 2023; Szkudlarek *et al.*, 2024). However, metal-based catalysts are generally expensive to synthesize. As a result, natural mineral-based catalysts such as calcium oxide (CaO) and magnesium oxide (MgO) have attracted growing attention due to their strong basicity, low solubility in methanol, low cost, and high reactivity (Bambase *et al.*, 2021; Marwaha *et al.*, 2018; Mazaheri *et al.*, 2021; Weldeslase *et al.*, 2023; Widiarti *et al.*, 2021). Calcium and magnesium are abundantly available in Indonesia, particularly in the Madura region. CaO is commonly derived from the decarbonation of natural dolomite or other calcium carbonate-rich sources such as eggshells, seashells, and fish bone waste.

In the Madura region of Indonesia, natural dolomite is abundantly available. However, pure CaO or MgO from dolomite has certain limitations, including low surface area and poor thermal stability (Yusuff *et al.*, 2022). To enhance catalytic activity, various studies have incorporated high-surface-area support materials for CaO-MgO such as silica, alumina, and zeolite. These supports help maintain good metal oxide dispersion, increasing the active site surface area. Hence, support materials for bifunctional catalysts have been widely investigated to improve basicity, thermal stability, and reusability (Tang *et al.*, 2018). Natural dolomite containing CaO-MgO has been combined with supports such as activated carbon (Sun *et al.*, 2021), fly ash (Pavlović *et al.*, 2020), mesoporous silica (De Lima *et al.*, 2014), and zeolite (Qu *et al.*, 2020).

Zeolite-based catalysts, especially those of the sodalite type, offer high basicity and are considered promising as catalyst supports. Sodalite-type zeolites can be synthesized using natural precursors such as kaolin, which is rich in Si and Al sources, and their synthesis involves relatively simple and short processing times. Yusuff et al investigated biodiesel production from used cooking oil via methanolysis using a CaO-zeolite composite catalyst synthesized from waste eggshells (Yusuff et al., 2022). The catalyst was synthesized via the wet impregnation method and subsequently calcined at temperatures between 700 and 900 °C. The optimum transesterification conditions were at a temperature of 69.1 °C for 238.8 minutes, catalyst loading of 2.1 wt% and methanol-tooil molar ratio of 9.7:1. A FAME (Fatty Acid Methyl Ester) yield of 93.7% was obtained. In a related study, Supamathanon et al developed a cost-effective heterogeneous base catalyst comprising CaO supported on modified geopolymer for transesterification of soybean oil (Supamathanon et al., 2021). The catalyst was synthesized via microwave irradiation followed by calcination at 600 °C. Incorporation of aluminum during geopolymer synthesis increased pore size, and the catalyst exhibited a 30%CaO/Geo FAME vield of  $93.12 \pm 0.48\%$ . markedly higher that of than 30%CaO/unfoamed-Geo, which yielded  $70.87 \pm 0.22\%$ .

Therefore, this study aims to develop a bifunctional sodalite-natural dolomite catalyst for biodiesel production, utilizing the high CaO-MgO content of natural dolomite. The bifunctional catalysts were synthesized with various dolomite loadings and evaluated for their catalytic activity in biodiesel production from CI oil via transesterification. Furthermore, the resulting biodiesel was also tested for its performance and emission characteristics in diesel engine.

## 2. Materials and Methods

## 2.1 Tools and Materials

The equipment used in this study includes a hotplate magnetic stirrer, beaker glass, analytical balance, three-neck round-bottom flask, water pump, condenser tube, hose, stirrer, thermometer, dropper, stand, centrifuge, separating funnel, tachometer, diesel engine, and burette. The materials employed were *Calophyllum Inophyllum* (CI) oil was obtained from Madura region, methanol (Merck), sulfuric acid (H<sub>2</sub>SO<sub>4</sub>, Smart Lab), sodium hydroxide (NaOH, Merck), sodium aluminate (Sigma Aldrich), methylheptadecanoate (Merck), natural kaolin, natural dolomite sourced from the Madura region, and demineralized water

#### 2.2 Synthesis of Sodalite

The synthesis process commenced by dissolving 4.47 g of sodium hydroxide pellets in 53 mL of demineralized water within a polypropylene container under continuous stirring. Subsequently, 6 g of kaolin was introduced into the NaOH solution and stirred until a homogeneous slurry was obtained. This was followed by the addition of 1.8 g of sodium aluminate, and the mixture was further stirred at ambient temperature for 24 hours. The resulting gel was aged at room temperature for an additional 24 hours before undergoing hydrothermal treatment at 100 °C for 24 hours. Upon completion, the mixture was cooled under running water, and the solid product was separated by filtration. The recovered solid was then dried at 100 °C for 24 hours to eliminate residual moisture.

#### 2.3 Synthesis of Natural Dolomite

Natural dolomite was initially crushed and sieved to obtain a particle size of 150 mesh. The sieved powder was then dried in an oven at 110  $^{\circ}$ C for 2 hours to eliminate moisture content. Subsequently, the dried material was subjected to calcination in a muffle furnace at 900  $^{\circ}$ C for 3 hours.

# 2.4 Synthesis of Bifunctional Sodalite-Natural Dolomite (SD) Catalyst

Initially, sodalite was weighed as much as 4.75 grams. Then 30 ml of distilled water was added and put into a beaker glass. Natural dolomite catalyst was then added as much as 0.25 grams into the mixture and stirred for 30 minutes at a speed of 400 rpm. The solid catalyst formed was filtered using filter paper, then dried using an oven at a 110 °C for 24 h. The catalyst was denoted as SD-5. The above procedure was then repeated with natural dolomite loading of 0.5; 0.75; 1 and 1.25 grams, each denoted as SD-10; SD-15; SD-20 and SD-25.

## 2.5 Catalyst Characterization

The synthesized catalyst solids were characterized using XRD, SEM-EDX, FTIR and  $N_2$  adsorption–desorption analysis. XRD analysis was performed using Cu  $K\alpha$  radiation with a Bruker D2 Phaser instrument over a  $2\theta$  range of  $5^\circ\text{--}80^\circ$  ( $\lambda=1.54056\ \mathring{A})$  to identify crystalline phases. FTIR spectra (Nicolet Avatar 360 IR) were obtained using KBr pellets in the wavenumber range of  $1400\text{--}400\ \text{cm}^{-1}$  to detect functional groups. SEM-EDX (Hitachi Flexsem 1000) was used to observe morphology, elemental mapping and composition. The samples were gold-coated for 150 seconds at 5 mA and  $6\times10^{-2}$  mbar pressure. Nitrogen adsorption–desorption analysis was carried out with a Quantachrome Novatouch Lx4 to determine surface area and pore size distribution.

#### 2.6 Biodiesel Production from CI Oil

#### 2.6.1 Esterification Stage

In this step, the esterification of CI oil was conducted using methanol and sulfuric acid  $(H_2SO_4)$  as homogeneous catalyst. The reaction was conducted using a methanol-to-oil

molar ratio of 9:1 with 4%  $\rm H_2SO_4$  (v/v) at 60 °C for 1 hour under continuous stirring at 600 rpm. Upon completion, the reaction mixture was placed in a separating funnel and left to stand undisturbed for 24 hours to allow phase separation, resulting in the formation of two distinct layers. The upper oil layer was collected and subsequently used in the transesterification process.

#### 2.6.2 Transesterification Stage

Transesterification of CI oil was carried out using methanol and SD-series catalysts. The reaction was performed in a three-neck round-bottom flask equipped with mechanical stirrer and reflux condenser. Initially, methanol was mixed with the SD-5 catalyst, followed by the gradual addition of the esterified oil. The reaction mixture was maintained at 65 °C for 2 h, catalyst loading of 2 wt.%, employing a methanol-to-oil molar ratio of 12:1. Upon completion, the biodiesel layer was separated using separating funnel, and the catalyst was recovered by centrifugation. The resulting biodiesel was analyzed using GC–MS. This procedure was repeated for the remaining catalysts (SD-10, SD-15, SD-20, and SD-25). The oil conversion and methyl ester yield were calculated based on Equations (1) and (2) (Maneerung *et al.*, 2016; Pansakdanon *et al.*, 2025; Widiarti *et al.*, 2021).

$$Oil conversion = \frac{Weight of initial oil - weight of residual}{Weight of initial oil} x 100 \% (1)$$

Metil ester yield = 
$$\left(\frac{\Sigma A_{ME}}{A_{is}}\right) \left(\frac{Cis \times Vis}{ms}\right) \times 100 \%$$
 (2)

Where  $\Sigma A_{ME}$ : Total peak area of methyl ester,  $A_{is}$ : Peak area of the internal standard,  $C_{is}$ : Concentration of the internal standard (g/mL),  $v_{is}$ : Volume of the internal standard (mL), ms: sample mass (mg).

#### 2.7 Performance and Emission Testing on Diesel Engine

The performance tests were conducted on TF 70LY-DI diesel engine coupled directly to an electric generator via the main shaft. The engine was modified for testing purposes by equipping it with a burette for measuring fuel consumption. The specifications of the diesel engine used in this study are shown in Table 1. The test setup is shown in Figure 1 and the schematic diagram of the installation is shown in Figure 2

The tests were conducted under a constant load (stationary load) condition, with engine speeds varying from 500 to 1500 rpm. Fuel was first introduced into the burette tube. The engine was then started, and the performance test was carried out by recording various parameters across different engine

Table 1

Diesel engine specifications	
Power Output	6.0 DK/2400 Rpm
Cylinder Capacity	382 cc
Number of Cylinders	1
Bore x Stroke (mm)	78 x 80
Spesific Fuel Consumtpion	175 g/HP.h
Engine type	TF 70LY-DI
Generator type	ST-3 Yamamoto
Power	3 Kw
Voltage	220 V
Current	13.6 A
Frequency	50 Hz
Rotational Speed	1500 rpm
Phase	Single phase
Power factor ( $\cos \varphi$ )	1.0

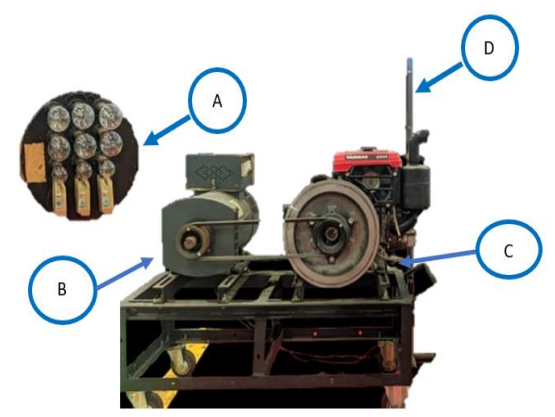


Fig. 1 Diesel engine testing tools

Description:
A. Load B. Generator C. Engine D. Burette tube

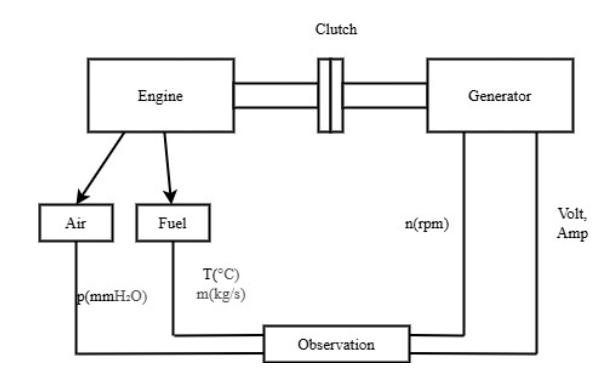


Fig. 2 Diesel Engine Testing Schematic Diagram

speeds. The observed parameters included fuel consumption (mL), time taken to consume the fuel (seconds), voltage (V), and current (A). Each test was repeated five times under different throttle valve openings while maintaining constant load conditions for each method. After data collection, the engine speed was gradually decreased to lower rpm. The engine was then allowed to run at no-load condition for approximately 5 minutes. Subsequently, the engine was turned off and allowed to cool. The remaining fuel was completely drained. The entire procedure was repeated using different fuel blend variations: B10, B20, B30, and B40.

### 3. Results and Discussion

The XRD diffractograms of catalyst samples with varying dolomite loadings are presented in Figure 3. The characteristic peaks of the sodalite phase were observed at 20 angles of approximately 13.94°, 24.29°, 31.80°, 35.00°, and 42.80° (Sari *et al.*, 2018). In contrast, calcium oxide (CaO) peaks result from the calcination of dolomite, which contains calcium carbonate (CaCO<sub>3</sub>). The calcination process facilitates the thermal decomposition of calcium carbonate into calcium oxide, accompanied by the release of carbon dioxide gas as a byproduct (Hamid *et al.*, 2023). The calcium hydroxide (Ca(OH)<sub>2</sub>) phase was detected at  $20 = 18.43^\circ$ , while calcium carbonate phases appeared at  $20 = 29.33^\circ$  and  $47.46^\circ$ . The characteristic peak of calcium oxide was observed at  $20 = 37.83^\circ$ . These diffractogram peaks are consistent with previous findings reported by Widiarti *et al.* (Widiarti *et al.*, 2024). All

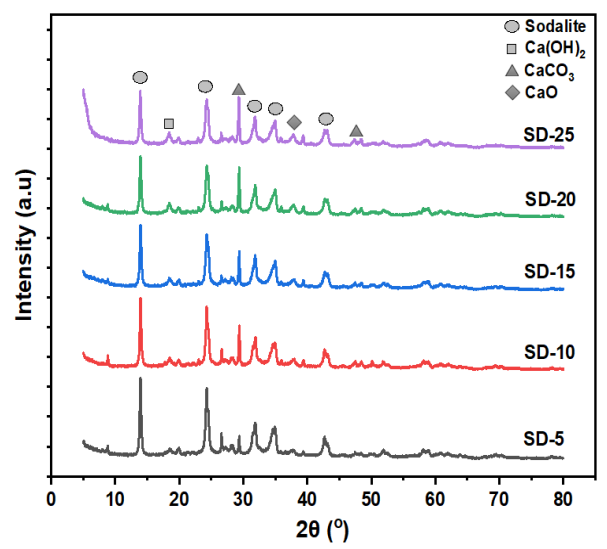


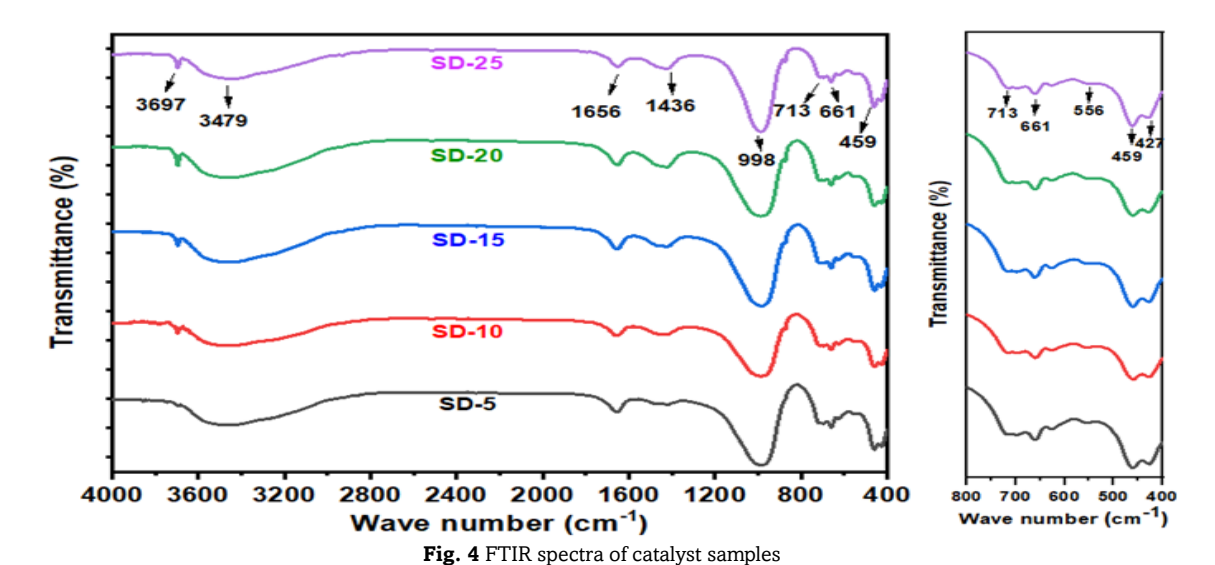
Fig. 3 Diffractogram of catalyst samples

samples exhibited similar diffraction patterns; however, increasing the dolomite loading led to higher peak intensities at  $2\theta=18.43^\circ$ ,  $29.33^\circ$ ,  $47.46^\circ$ , and  $37.83^\circ$ , indicating that the SD-25 catalyst contains higher proportions of CaO and CaCO $_3$  phases compared to the other catalysts. Conversely, the intensity of the sodalite phase decreased with increased dolomite loading. This phenomenon is attributed to the impregnation process of dolomite into the sodalite pores, which occurs through precursor solution diffusion, ion adsorption, drying, and calcination allowing the dolomite compounds to be dispersed within the sodalite structure.

FTIR analysis was conducted to identify the atomic bonding and molecular vibrations within the catalyst samples. The FTIR spectra of the catalyst samples are presented in Figure 4. The catalyst samples exhibited characteristic FTIR spectra of sodalite, as indicated by a peak at 998 cm<sup>-1</sup> corresponding to the asymmetric stretching vibration of T–O–T bonds (where T = Silica or Aluminium) within the sodalite framework (Wahyuni *et al.*, 2019). The Peaks observed at 713 and 661 cm<sup>-1</sup> were attributed to the symmetric stretching vibration of T–O–T, while the absorption band at 556 cm<sup>-1</sup> corresponded to Al–O deformation. A peak at 461 cm<sup>-1</sup> indicated Si–O bending vibrations, whereas the presence of

single 4-membered rings of the sodalite structure was confirmed by bands in the 427–459 cm<sup>-1</sup> region (Ulfa *et al.*, 2022). The spectra also revealed several other notable features, including a sharp peak at 3697 cm<sup>-1</sup> and broad band around 3479 cm<sup>-1</sup>, which are associated with O–H stretching vibrations from water and Ca(OH)<sub>2</sub> (Olutoye *et al.*, 2016; Widiarti *et al.*, 2021). Additionally, absorption bands within the range of 1436–1656 cm<sup>-1</sup> were identified, indicating the presence of carbonate groups (Lawan *et al.*, 2020). These results are consistent with previous FTIR data reported for CaO-based catalysts derived from eggshell supported on zeolite for biodiesel production (Yusuff *et al.*, 2022).

The absence of the peak at 3697 cm<sup>-1</sup> in the SD-5 sample suggests that only a small amount of CaO was dispersed on the sodalite surface. Furthermore, the intensity of the peak at 1436 cm<sup>-1</sup> increased significantly, particularly in the SD-25 sample, indicating a higher concentration of carbonate groups. This observation correlates with the higher dolomite loading in the SD-25 sample compared to the other catalysts. The results of the morphological analysis, elemental mapping composition of the catalyst samples using SEM-EDX are presented in Figure 5 and Table 2. The morphology of all samples appeared relatively similar, forming irregularly shaped, agglomerated spherical particles with an average particle size of approximately 500 nm. Based on SEM-EDX analysis of sodalite catalysts modified with 5-25% natural dolomite loading, variations in elemental composition were observed, reflecting structural and mineralogical changes within the catalyst material. Oxygen (O) remained the dominant element across all samples, ranging from 43.11% to 46.39% by weight, indicating the stable presence of oxides such as silicates, aluminates, and carbonates within the material framework. Aluminum (Al), a key element in the sodalite framework, showed a slight decrease from 17.19% (SD-10) to 15.39% (SD-25). Similarly, the silicon (Si) content also decreased from 17.66% (SD-10) to 14.84% (SD-25). This reduction suggests possible substitution or dilution of the sodalite crystal structure by dolomite components, particularly at higher dolomite ratios. Magnesium (Mg) and calcium (Ca), which are the primary constituents of dolomite (CaMg(CO<sub>3</sub>)<sub>2</sub>), exhibited a clear increasing trend with higher dolomite loadings. Mg content increased significantly from 1.38% in SD-5 to 5.53% in SD-15, while Ca increased from 1.14% (SD-5) to 4.61% (SD-25). Overall, this quantitative analysis indicates that gradual incorporation of natural dolomite successfully modified the chemical composition of the sodalite



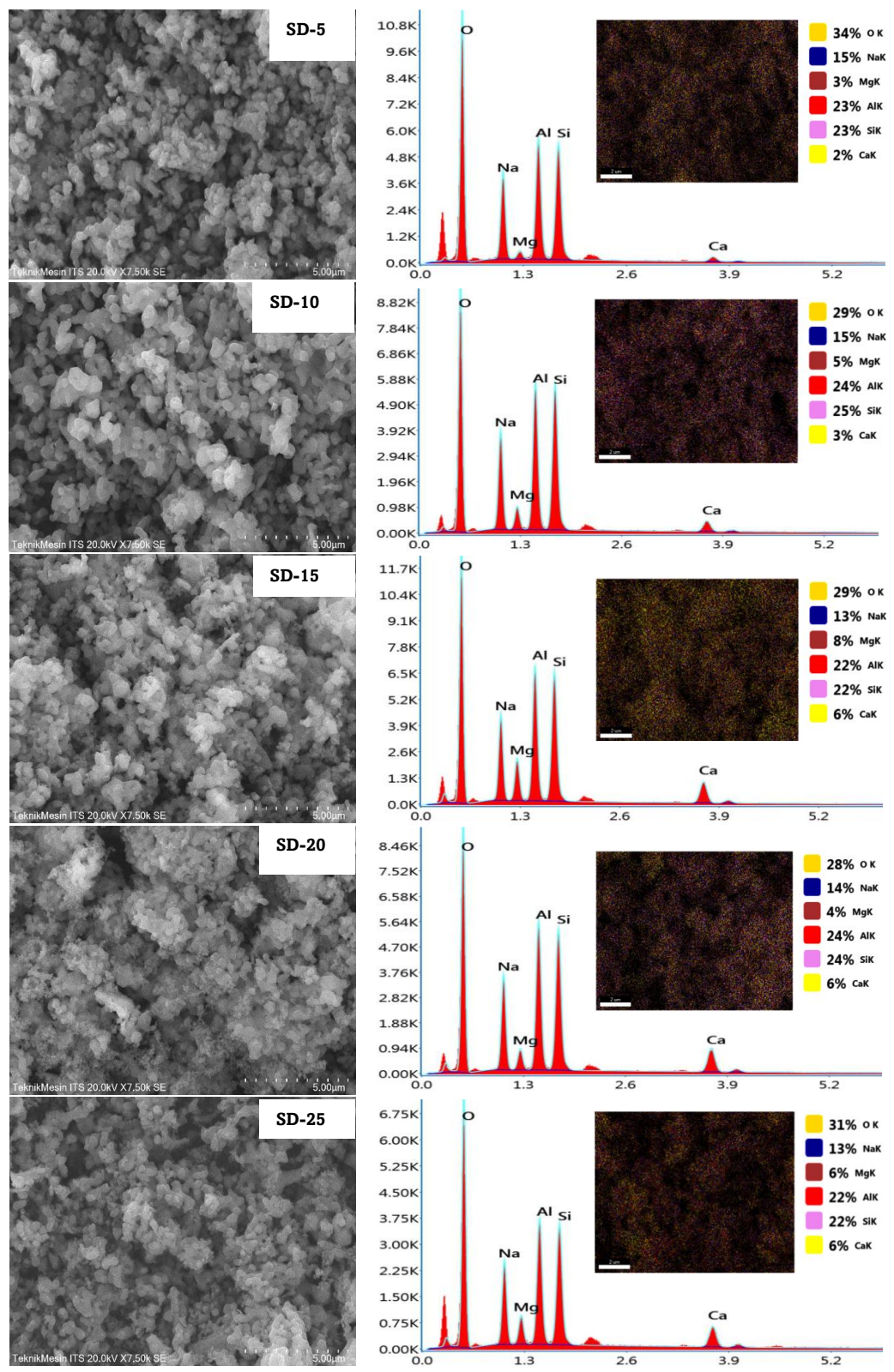


Fig. 5 SEM analysis and elemental mappings of catalyst sample

catalyst by enriching it with Mg and Ca, while slightly reducing Al and Si content, which may influence the catalytic basicity and activity.

The  $N_2$  adsorption–desorption isotherms of all catalyst samples are presented in Figure 6. Samples SD-5, SD-10, and SD-15 exhibited combination of type II and IV isotherms, indicating relatively low surface area and mesoporosity. In contrast, catalysts SD-20 and SD-25 showed an increase in

surface area and porosity, as evidenced by the broader hysteresis loops in the isotherm curves compared to other samples, suggesting the presence of mesoporous characteristics with type IV isotherms (Ediati  $et\ al.$ , 2025). The analysis results revealed a combination of microporous and mesoporous surface areas, as presented in Table 3, with dominant mesoporous surface area of 17.936 m²/g and total surface area of 20.901 m²/g. The presence of the hysteresis loop is attributed

 Table 2

 Elemental content from SEM-EDX analysis of catalyst

_	Elemental content (% wt)					
Catalyst	0	Na	Mg	Al	Si	Ca
SD-5	46,39	17,98	1,38	16,66	16,44	1,14
SD-10	43,11	16,70	3,16	17,19	17,66	2,19
SD-15	44,88	14,63	5,53	15,67	15,19	4,10
SD-20	44,27	15,86	2,76	16,51	16,05	4,55
SD-25	45,81	15,29	4,06	15,39	14,84	4,61

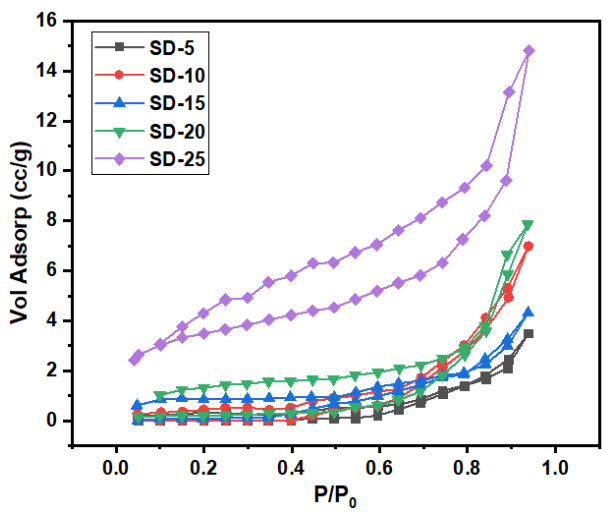


Fig. 6 Isotherm graph of catalyst samples

to capillary condensation within the mesopores (Hamid *et al.*, 2023). This observation is supported by the data in Table 3, where the SD-25 catalyst exhibited the highest. The table summarizes the surface area and pore structure characterization results of the catalysts, as determined by  $N_2$  adsorption–desorption analysis at various dolomite loadings. The results indicate that increasing dolomite loading generally enhances the BET surface area (S-BET), implying that a higher dolomite content leads to larger specific surface area of the catalyst. The highest surface area was observed in the SD-25 catalyst, reaching 20.901  $m^2/g$ . This suggests that dolomite addition contributes to the development of more complex pore structure.

At low dolomite loadings (SD-5 and SD-10), mesopores contributed more significantly than micropores. However, in the SD-15 samples, the micropore surface area (7.538  $\rm m^2/g)$  became dominant, indicating the possible formation of microporous structures due to interactions between dolomite and the base material. In contrast, for the SD-25 catalyst, mesoporosity became dominant once again (17.936  $\rm m^2/g)$ , accompanied by an increase in both the average pore diameter and the total pore volume

The catalytic performance of natural dolomite with varying loadings was evaluated in the transesterification of CI oil at 65 °C for 2 hours, employing a methanol-to-oil molar ratio of 12:1. The catalyst dosage was maintained at 2 wt.% relative to the oil. Biodiesel yield was determined using GC-MS analysis, as shown in Figure 7. The biodiesel yield increased significantly from 81.04% to 89.45% with an increase in dolomite catalyst loading from 5% to 10%. Further increases in dolomite loading up to 25% resulted in a slight improvement in yield. The biodiesel yields for catalysts SD-20 and SD-25 were 93.79% and 94.14%, respectively, indicating only a marginal difference. The enhanced catalytic activity is attributed to the high CaO content

Table 3

Physicoche Physicoche	emical proper	erties of catalyst samples				
Sample	$S_{BET}(m^2/g)$	$S_{micro}$	$S_{meso}$	Average	Vol total	
		$(m^2/g)$	$(m^2/g)$	Pore	(cc/nm/g)	
				size		
				(nm)		
SD-5	7,696	3.452	4,244	1,90	0,005	
SD-10	8,155	3.232	4,923	3,68	0,005	
SD-15	11,643	7.538	4,105	5,06	0,006	
SD-20	12,233	5.425	6,808	5,46	0,006	
SD-25	20,901	2.965	17,936	5,86	0,023	

in the SD-25 catalyst, particularly due to the strong basic properties of CaO active sites, which facilitate the formation of methoxide anions from methanol. In addition, the higher surface area and mesoporosity of SD-25 also contribute to its improved catalytic performance. As a reactive nucleophilic species, the methoxide anion attacks the electrophilic carbonyl carbon in triglycerides to form biodiesel (Shalihah et al., 2020). The presence of calcium oxides in the catalyst structure significantly influences its alkalinity (Gomes et al., 2012; Marinković et al., 2017), which is attributed to the Ca metal ions, as one of the initial elements in the alkaline earth metal group, it enhances the electron density on oxygen atoms, thereby increasing catalytic efficiency in the base-catalyzed hydrolysis mechanism (Rabie et al., 2019). Additionally, it contributes to the stabilization of polarized species, such as calcium or magnesium methoxides and fatty acid salts, which in turn improves biodiesel yield. The highest conversion of CI oil to biodiesel was achieved using the SD-25 catalyst. High natural dolomite loading, which provides a strong basic CaO content, tends to result in higher biodiesel conversion.

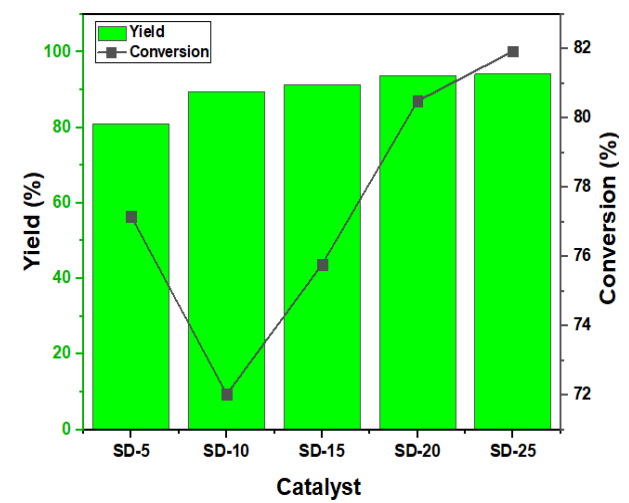


Fig. 7 Metil ester yield and conversion of biodiesel

**Table 4** Properties of biodiesel

No	Parameter	Results	Test Method	Standard	
				(ASTM D6751)	
1	Flash point	192 °C	ASTM D92	Min 130	
2	Kinematic Viscosity at 40 °C	7.13 cst	ASTM D445	1.9-6	
3	Density at 15 °C	898 kg/m <sup>3</sup>	Picnometer	860-900	
4	Acid number	0.14 mg-KOH/g	SNI 7182:2015	Max 0.5	

Table 4 presents the physicochemical characteristics of the produced biodiesel. The initial parameter presented is the flash point, defined as the lowest temperature at which fuel vapors ignite upon exposure to an ignition source (Nguyen et al., 2023). The biodiesel exhibited a flash point of 192 °C, significantly higher than the ASTM minimum requirement of 101 °C. This indicates lower volatility compared to fossil fuels such as conventional diesel. The kinematic viscosity at 40 °C, which reflects the fluid's resistance to flow, was measured at 7.13 cSt slightly exceeding the ASTM standard range of 3.5-5.0 cSt. However, the biodiesel density was found to be 898 kg/m3, falling within the acceptable standard range of 860-900 kg/m<sup>3</sup>, suggesting good fuel stability and compatibility with diesel engine specifications. Furthermore, the acid value of the biodiesel was relatively low at 0.14 mg-KOH/g, indicating minimal free fatty acid content, which reduces the risk of corrosion in engine components (Yang et al., 2016).

The FTIR spectrum of biodiesel produced from CI oil is illustrated in Figure 8. The broad absorption band observed at 3478 cm<sup>-1</sup> corresponds to O–H stretching vibrations. The distinct peaks at 2921 cm<sup>-1</sup> and 2856 cm<sup>-1</sup> are attributed to the asymmetric and symmetric stretching vibrations of C–H bonds within the CH<sub>2</sub> and CH<sub>3</sub> groups, respectively. The prominent absorption at 1746 cm<sup>-1</sup> is characteristic of the C=O stretching vibration associated with the triglyceride ester linkage (Nisar *et al.*, 2017). Bands appearing at 1464 cm<sup>-1</sup> and 1377 cm<sup>-1</sup> are assigned to H–CH and CH<sub>2</sub> bending vibrations. The absorption peak at 1169 cm<sup>-1</sup> corresponds to the C–O stretching vibration of the ester functional group, while the band at 725 cm<sup>-1</sup> is indicative of bending vibrations of the (CH<sub>2</sub>)<sub>n</sub> group (Shalaby & Sh El-Gendy, 2012).

The transesterification reaction mechanism for biodiesel production using bifunctional sodalite-natural dolomite catalyst is illustrated in Figure 9. Sodalite acts as a promising basic catalyst due to the presence of two primary active sites, namely  $Na^+$  and  $K^+$  ions. Upon impregnation with dolomite, these active sites can be substituted by  $Ca^{2^+}$  and  $Mg^{2^+}$  ions (Fig. 9). In

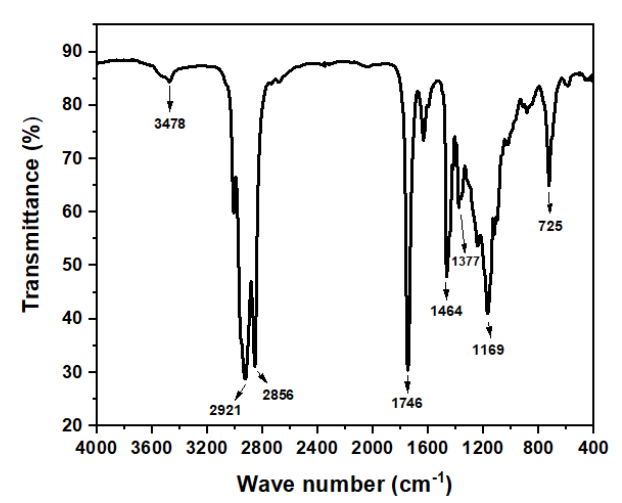


Fig. 8 FTIR spectra of biodiesel sample

general, the reaction pathway is influenced by the catalytic properties of the material, in which the incorporation of calcium and magnesium ions enhances the basic character of the active sites. At the initial stage, methanol molecules are adsorbed onto the surface of the sodalite catalyst. During this process, protonation of the hydrogen atom in methanol occurs, followed by ion exchange between the methanol and metal ions (Ca2+/Mg2+), leading to the formation of an alkoxide anion (CH<sub>3</sub>O<sup>-</sup>). Simultaneously, fatty acids are effectively adsorbed onto the catalyst surface through siloxane groups in the sodalite structure, which act as oxygen donors and interact with the carbonyl functional groups. The generated CH<sub>3</sub>O<sup>-</sup> anion then attacks the protonated carbonyl group, resulting in the formation of methyl ester compounds as the final reaction products. The formation of methoxide groups on the sodalite surface is facilitated by the acidity of the adsorbed methanol and stabilized by the basic sites and their interaction with the acidic sites in the sodalite framework. These acidic sites originate from the oxygen atoms within the silica tetrahedra and alumina octahedra that constitute the sodalite structure.

Figure 10 illustrates the torque values at various engine speeds (rpm) for different biodiesel fuel blend variations. The figure shows how the biodiesel content in the fuel influences engine torque across a range of engine speeds. In general, torque increases with engine speed, reaching its peak at 1250 rpm. At around 500 rpm, the torque values are relatively low for all fuel types. The lower torque observed at low speed in internal combustion engines (ICE) is due to the fact that maximum torque is typically achieved at a lower engine speed than maximum power output. At initial engine speeds, the torque is lower due to the engine's volumetric efficiency characteristics. When the engine is under load (acceleration), it must work harder to maintain the same speed. This indicates that the engine needs to convert more fuel into energy to produce the required output power. Since the available energy from the fuel is limited, the engine slows down to sustain the necessary output.

Interestingly, the B20 fuel blend achieved the highest torque value (8.713 N.m), while B10 and B40 blends exhibited lower torque values compared to pure diesel (D100). This suggests that at low engine speeds, biodiesel content has minimal influence on torque. However, there is a tendency for certain biodiesel proportions to result in more optimal combustion. In the medium speed range (750-1000 rpm), fuel blends with higher biodiesel content (B40) produced greater torque than pure diesel. For instance, at 750 rpm, B40 generated the highest torque of 35.029 N.m, surpassing D100 at 31.441 N.m. Similarly, at 1000 rpm, B40 produced the highest torque at 62.991 N.m, significantly higher than the other fuel variations. This indicates that at medium engine speeds, high biodiesel content enhances combustion efficiency, likely due to the oxygenated nature of biodiesel that supports better combustion. However, at high engine speed (1250 rpm), the torque differences among fuel types became less pronounced. The highest torque at this speed was achieved with B10 at 69.151 N.m, slightly higher than D100 and B40, which recorded 67.794 and 67.251 N.m, respectively. This suggests that at high speed, the influence of biodiesel content on torque diminishes, possibly

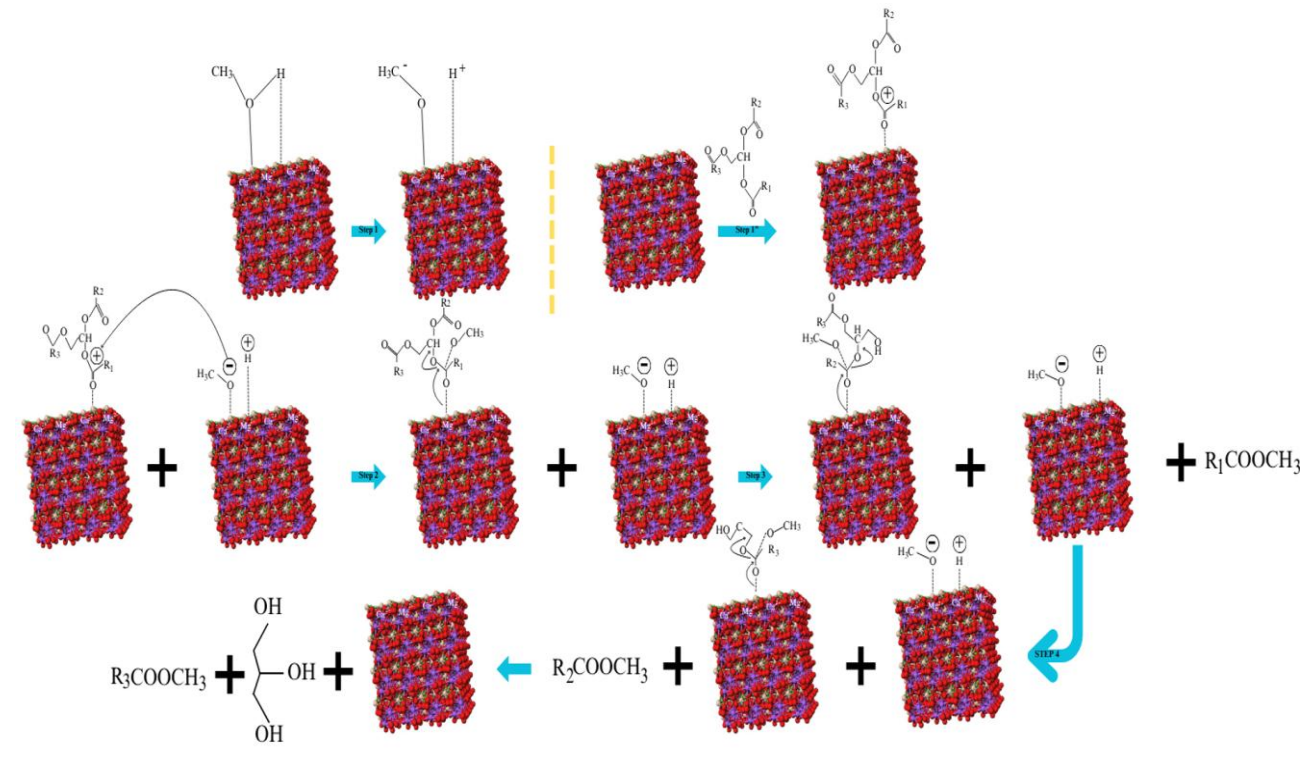


Fig. 9 Transesterification reaction mechanism of WCO using bifunctional sodalite-natural dolomite catalyst

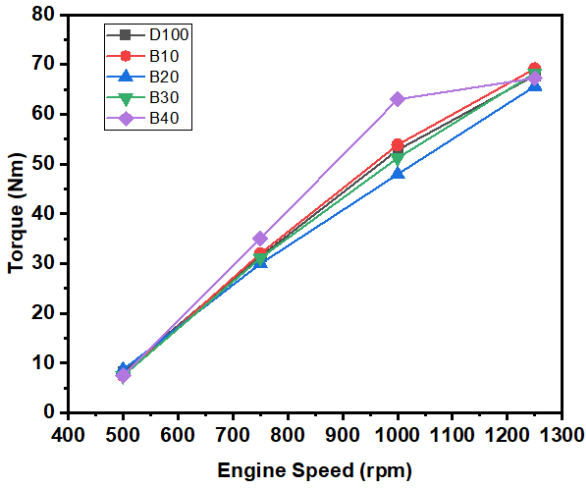


Fig. 10 Torque value of fuel blends

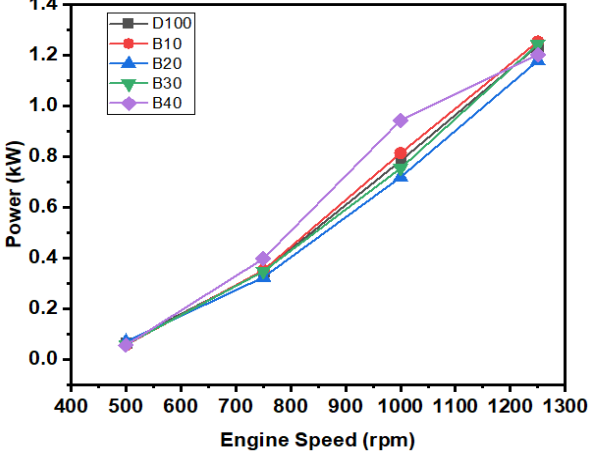


Fig. 11 Power value of fuel blends

due to decreasing volumetric efficiency of the engine. Overall, the use of biodiesel can affect engine torque, particularly at medium engine speeds, where higher biodiesel content may provide better performance than pure diesel.

The power output results of the fuel blend variations are presented in Figure 11. At an engine speed of 500 rpm, the D100 fuel produced the highest power output, recorded at 0.099 kW, compared to all biodiesel blends. In the case of the B10 blend, the power output at 500 rpm was lower than that of D100. However, as engine speed increased, the power output also gradually approaching the increased. performance characteristics of D100. At 1250 rpm, the B10 fuel began to exhibit a decline in power, likely due to incomplete combustion processes. For B20 and B30 blends, the power output remained below that of D100 across the tested engine speeds, although the performance of B20 was closest to that of pure diesel. The maximum to minimum power outputs at 1250 rpm were observed for B10 (1.252 kW), B30 (1.242 kW), D100 (1.235 kW), B50 (1.200 kW), B40, and B20 (1.177 kW), respectively. Biodiesel typically has a lower calorific value than conventional diesel, resulting in reduced energy conversion into mechanical power and, consequently, a slight decrease in output power (Buyukkaya, 2010). Nonetheless, differences in power output among biodiesel blend ratios were not significant at lower engine speeds. This phenomenon may be attributed to the slower combustion rate of biodiesel compared to conventional diesel and its higher viscosity, which can negatively impact combustion efficiency within the engine cylinder (Mengistu *et al.*, 2024).

The specific fuel consumption (SFC) test results of the fuel blends are presented in Figure 12. At low engine speed, around 500 rpm, the highest Specific Fuel Consumption (SFC) was observed for the B40 biodiesel blend at 0.0026 kg/kWh, while the lowest SFC was recorded for B20 at 0.0017 kg/kWh. This indicates that at low speed, higher biodiesel content tends

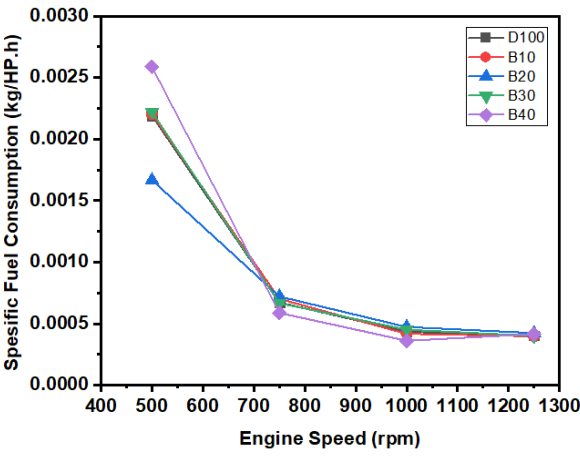


Fig. 12 SFC value of fuel blends

to increase fuel consumption. The primary factor influencing this behavior is the higher viscosity of biodiesel compared to pure diesel, which can affect fuel atomization and combustion efficiency (How et al., 2018). At medium engine speeds, approximately 750-1000 rpm, the specific fuel consumption becomes more uniform across the different fuel types. At 750 rpm, all fuel types exhibited similar SFC values of about 0.0007 kg/kWh, with a slight decrease for B40 at 0.0006 kg/kWh. At 1000 rpm, the differences in SFC among the fuel variations were relatively small, ranging from 0.0004 to 0.0005 kg/kWh. This suggests that combustion becomes more stable and efficient at medium speeds, thereby reducing the impact of biodiesel content variation on fuel consumption. At high engine speed, around 1250 rpm, all fuel blends exhibited the same specific fuel consumption of 0.0004 kg/kWh. This indicates that at high speed, the engine reaches optimal efficiency, where differences in fuel characteristics, such as viscosity and calorific value, no longer significantly affect specific fuel consumption. Therefore, the use of biodiesel can offer fuel efficiency comparable to pure diesel at high engine speeds, although higher fuel consumption may still occur at lower speeds, especially with blends containing higher biodiesel content.

Figure 13 presents the carbon monoxide (CO) emission levels for various biodiesel fuel blends. The emission results show a decreasing trend in CO emissions with increasing biodiesel content in the fuel blend. This is attributed to the chemical properties of biodiesel, which contains a higher oxygen content compared to pure diesel fuel (D100). The elevated oxygen content in biodiesel enhances combustion efficiency, thereby reducing the formation of CO, which is

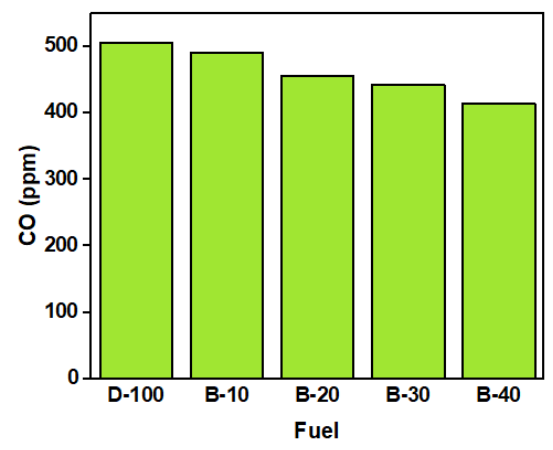


Fig. 13 CO gas content of the fuel blends

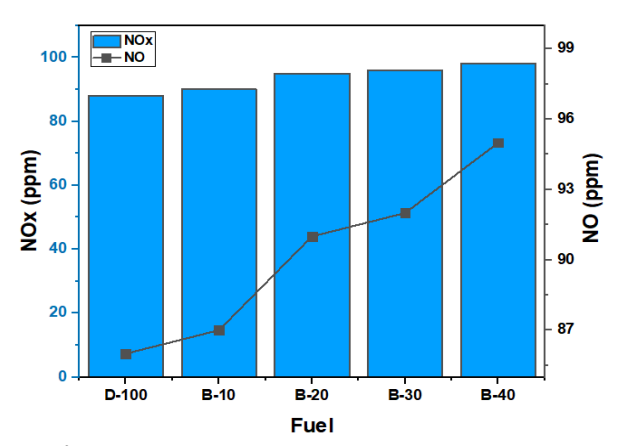


Fig. 14 NO and NO<sub>x</sub> gases content of the fuel blends

typically produced because of incomplete combustion (Chen *et al.*, 2023). CO emissions are generated through the oxidation of carbon atoms in the fuel (Jamshaid *et al.*, 2022). Pure diesel (D100) produced the highest CO emissions at 505 ppm, followed by B10, B20, B30, and B40, with emission levels of 490 ppm, 455 ppm, 442 ppm, and 414 ppm, respectively. The use of B40 resulted in a CO emission reduction of approximately 18.02%. This demonstrates that biodiesel plays a significant role in reducing CO emissions during the engine combustion process.

The emission test results for NO and NO<sub>x</sub> gases, as shown in Figure 14, indicate an increasing trend with the rising percentage of biodiesel in the fuel blends. Pure diesel (D100) produced the lowest NOx and NO emissions, recorded at 88 ppm and 86 ppm, respectively. In contrast, the biodiesel blend with the highest proportion (B40) exhibited increased NOx and NO emissions, reaching up to 98 ppm and 95 ppm, respectively. This suggests that the use of biodiesel tends to increase nitrogen oxide (NO<sub>x</sub>) emissions, including nitrogen monoxide (NO). The increase in NOx and NO emissions with biodiesel blends can be attributed to the combustion characteristics of biodiesel. Biodiesel exhibits a greater oxygen content relative to conventional diesel fuel. This additional oxygen enhances combustion efficiency and results in higher combustion temperatures. Elevated combustion temperatures contribute to greater NO<sub>x</sub> formation, as nitrogen in the intake air reacts with oxygen at high temperatures in the combustion chamber (Chen et al., 2023).

#### 4. Conclusion

Bifunctional catalysts based on sodalite and natural dolomite can be efficiently utilized for biodiesel production from CI oil. Physicochemical characterization results indicated that the catalyst with 25% dolomite loading (SD-25) exhibited the highest mesoporous area and pore volume, along with an optimal CaO content. The SD-25 catalyst demonstrated the best catalytic performance, achieving a maximum biodiesel yield of 94.14%. Experimental studies on diesel engine revealed that the B10 fuel blend produced the highest power and torque at 1250 rpm, reaching 1.252 kW and 69.151 N.m, respectively. While the B40 blend resulted in the lowest CO emissions at 414 ppm. However, NO and NO $_{\rm x}$  emissions tended to increase with higher biodiesel content. These findings highlight the significant potential of utilizing locally sourced minerals as catalyst materials for sustainable energy applications.

#### Acknowledgments

The authors would like to express their gratitude to Politeknik Negeri Madura for providing research funding through the 2024 Vocational Product Research Scheme. The authors also extend their appreciation to Institut Teknologi Sepuluh Nopember for their collaboration and support.

**Author Contributions**: MF: Conceptualization, methodology and formal analysis, AH: supervision, writing—original draft resources, validation and conceptualization, ZR: writing—review, validation and supervision, S: Data analysis, TEB: project administration and validation, AJ: Editing and validation. All authors have read and agreed to the published version of the manuscript.

**Funding:** This research was funded by Politeknik Negeri Madura under research contract number: 1143/PL34/AL.04/2024.

Conflicts of Interest: The authors declare no conflict of interest.

#### References

- Abdul Hakim Shaah, M., Hossain, M. S., Salem Allafi, F. A., Alsaedi, A., Ismail, N., Ab Kadir, M. O., & Ahmad, M. I. (2021). A review on non-edible oil as a potential feedstock for biodiesel: physicochemical properties and production technologies. *RSC Advances*, 11(40), 25018–25037. https://doi.org/10.1039/d1ra04311k
- Afsharizadeh, M., & Mohsennia, M. (2021). Novel rare-earth metal oxides-zirconia nanocatalysts for biodiesel production from corn oil and waste cooking oil. *Fuel*, *304*(June), 121350. https://doi.org/10.1016/j.fuel.2021.121350
- Aparamarta, H. W., Gunawan, S., Ihsanpuro, S. I., Safawi, I., Bhuana, D. S., Mochtar, A. F., & Yusril Izhar Noer, M. (2022). Optimization and kinetic study of biodiesel production from nyamplung oil with microwave-assisted extraction (MAE) technique. *Heliyon*, 8(8), e10254. https://doi.org/10.1016/j.heliyon.2022.e10254
- Aparamarta, H. W., Hapsari, S., Gunawan, S., Shiena, R. I., Ariandi, A. G., & Ju, Y. H. (2019). The election of edible and non edible crop for biodiesel feedstock in Indonesia with AHP-BCR and GC analysis. *Malaysian Journal of Fundamental and Applied Sciences*, 15(5), 767-771. https://doi.org/10.11113/mifas.v15n5.1440
- Azhar, B., Gunawan, S., Muharja, M., Avian, C., Satrio, D., & Aparamarta, H. W. (2024). Optimization of microwave-assisted extraction in the purification of triglycerides from non-edible crude Calophyllum inophyllum oil as biodiesel feedstock using artificial intelligence. *South African Journal of Chemical Engineering*, 47, 312–321. https://doi.org/10.1016/j.sajce.2023.12.001
- Bambase, M. E., Almazan, R. A. R., Demafelis, R. B., Sobremisana, M. J., & Dizon, L. S. H. (2021). Biodiesel production from refined coconut oil using hydroxide-impregnated calcium oxide by cosolvent method. *Renewable Energy*, 163, 571–578. https://doi.org/10.1016/j.renene.2020.08.115
- Brahma, S., Nath, B., Basumatary, B., Das, B., Saikia, P., Patir, K., & Basumatary, S. (2022). Biodiesel production from mixed oils: A sustainable approach towards industrial biofuel production. *Chemical Engineering Journal Advances, 10*(January), 100284. https://doi.org/10.1016/j.ceja.2022.100284
- Buchori, L., Widayat, W., Norzita, N., Hadiyanto, H., Okvitarini, N. (2024). Preparation of KI/KIO3/Methoxide Kaolin Catalyst and Performance Test of Catalysis in Biodiesel Production. Science and Technology Indonesia, 9 (2), 359 370. https://doi.org/10.26554/sti.2024.9.2.359-370
- Buyukkaya, E. (2010). Effects of biodiesel on a di diesel engine performance, emission and combustion characteristics. *Fuel*, 89(10), 3099–3105. https://doi.org/10.1016/j.fuel.2010.05.034
- Chen, Y., Zhang, J., Zhang, Z., Zhong, W., Zhao, Z., & Hu, J. (2023). Utilization of renewable biodiesel blends with different proportions for the improvements of performance and emission characteristics of a diesel engine. *Heliyon*, 9(9), e19196. https://doi.org/10.1016/j.heliyon.2023.e19196

- Darwin, Thifal, M., Alwi, M., Murizal, Z., Pratama, A., & Rizal, M. (2023).

  The synthesis of biodiesel from palm oil and waste cooking oil via electrolysis by various electrodes. *Case Studies in Chemical and Environmental Engineering*, 8(July), 100512. https://doi.org/10.1016/j.cscee.2023.100512
- De Lima, A. L., Mbengue, A., San Gil, R. A. S., Ronconi, C. M., & Mota, C. J. A. (2014). Synthesis of amine-functionalized mesoporous silica basic catalysts for biodiesel production. *Catalysis Today*, 226, 210–216. https://doi.org/10.1016/j.cattod.2014.01.017
- de S. Barros, S., Pessoa Junior, W. A. G., Sá, I. S. C., Takeno, M. L., Nobre, F. X., Pinheiro, W., Manzato, L., Iglauer, S., & de Freitas, F. A. (2020). Pineapple (Ananás comosus) leaves ash as a solid base catalyst for biodiesel synthesis. *Bioresource Technology*, 312(May), 123569. https://doi.org/10.1016/j.biortech.2020.123569
- Ediati, R., Putra Hidayat, A. R., Syukrie, T. D., Zulfa, L. L., Jannah, M., Harmami, H., Fansuri, H., & Ibnu Ali, B. T. (2025). Investigation the adsorption kinetic and isotherm studies of Remazol Red 5B dye on benzoic acid modified Al2O3/UiO-66 composite. In *Arabian Journal of Chemistry* (Vol. 18, Issue 1). Elsevier B.V. https://doi.org/10.1016/j.arabjc.2024.106078
- Emeji, I. C., & Patel, B. (2024). Box-Behnken assisted RSM and ANN modelling for biodiesel production over titanium supported zincoxide catalyst. *Energy*, 308. https://doi.org/10.1016/j.energy.2024.132765
- Fauzan, N. A., Tan, E. S., Pua, F. L., & Muthaiyah, G. (2020). Physiochemical properties evaluation of Calophyllum inophyllum biodiesel for gas turbine application. South African Journal of Chemical Engineering, 32, 56–61. https://doi.org/10.1016/j.sajce.2020.02.001
- Fiala, K., Thongjarad, A., & Leesing, R. (2024). Valorization of durian peel as a carbon feedstock for a sustainable production of heterogeneous base catalyst, single cell oil and yeast-based biodiesel. *Carbon Resources Conversion*, 7(3), 100224. https://doi.org/10.1016/j.crcon.2024.100224
- Gamboa, D., Herrera, B., Acevedo, J., López, D., & Cacua, K. (2024).

  Experimental evaluation of a diesel engine using amidefunctionalized carbon nanotubes as additives in commercial diesel and palm-oil biodiesel. *International Journal of Thermofluids*, 22(April).

  https://doi.org/10.1016/j.ijft.2024.100669
- Gomes, J. F. P., Puna, J. F. B., Bordado, J. C. M., Correia, M. J. N., & Dias, A. P. S. (2012). Status of biodiesel production using heterogeneous alkaline catalysts. *International Journal of Environmental Studies*, 69(4), 635–653. https://doi.org/10.1080/00207233.2012.693286
- Hamid, A., Jakfar, A., Romaniyah, S. B., Febriana, I. D., Abdullah, M.,
   Rahmawati, Z., & Prasetyoko, D. (2023). Transesterification of
   Waste Cooking Oil using CaO Catalyst Derived from Madura
   Limestone for Biodiesel Production and Its Application in Diesel
   Engine. Automotive Experiences, 6(1), 80–93.
   https://doi.org/10.31603/ae.7879
- Hamid, A., Nugraha, R. E., Holilah, H., Bahruji, H., & Prasetyoko, D. (2023a). Large intraparticle mesoporosity of hierarchical ZSM-5 synthesized from kaolin using silicalite seed: effect of aging time and temperature. *Journal of the Korean Ceramic Society*, 60(2), 344–356. https://doi.org/10.1007/s43207-022-00267-0
- Hazmi, B., Rashid, U., Moser, B. R., Ab Ghani, M. H., Alharthi, F. A., Han, J., & Yoo, J. (2025). Environmentally sustainable production of biodiesel from low-cost lipid feedstock using a zirconium-based metal-organic framework sulfonated solid catalyst. Green Chemical Engineering. https://doi.org/10.1016/j.gce.2024.10.001
- How, H. G., Masjuki, H. H., Kalam, M. A., Teoh, Y. H., & Chuah, H. G. (2018). Effect of Calophyllum Inophyllum biodiesel-diesel blends on combustion, performance, exhaust particulate matter and gaseous emissions in a multi-cylinder diesel engine. Fuel, 227, 154–164. https://doi.org/10.1016/j.fuel.2018.04.075
- Hussain, J., Ali, Z. M., Qureshi, K. M., Khawaja, N., & Shah, S. F. A. (2022). Production of Biodiesel from Jatropha Curcas by using Heterogenous Dopped Zinc Oxide. *JOURNAL OF NANOSCOPE* (JN), 3(2), 173–182. https://doi.org/10.52700/jn.v3i2.78
- Jamshaid, M., Masjuki, H. H., Kalam, M. A., Zulkifli, N. W. M., Arslan, A., & Qureshi, A. A. (2022). Experimental investigation of performance, emissions and tribological characteristics of B20

- blend from cottonseed and palm oil biodiesels. *Energy*, 239. https://doi.org/10.1016/j.energy.2021.121894
- Kalita, P., Basumatary, B., Saikia, P., Das, B., & Basumatary, S. (2022). Biodiesel as renewable biofuel produced via enzyme-based catalyzed transesterification. *Energy Nexus*, 6(December 2021), 100087. https://doi.org/10.1016/j.nexus.2022.100087
- Lawan, I., Garba, Z. N., Zhou, W., Zhang, M., & Yuan, Z. (2020). Synergies between the microwave reactor and CaO/zeolite catalyst in waste lard biodiesel production. *Renewable Energy*, 145, 2550–2560. https://doi.org/10.1016/j.renene.2019.08.008
- Maneerung, T., Kawi, S., Dai, Y., & Wang, C. H. (2016). Sustainable biodiesel production via transesterification of waste cooking oil by using CaO catalysts prepared from chicken manure. *Energy Conversion and Management*, 123, 487–497. https://doi.org/10.1016/j.enconman.2016.06.071
- Marinković, D. M., Avramović, J. M., Stanković, M. V., Stamenković, O. S., Jovanović, D. M., & Veljković, V. B. (2017). Synthesis and characterization of spherically-shaped CaO/Γ-Al2O3 catalyst and its application in biodiesel production. *Energy Conversion and Management*, 144, 399–413. https://doi.org/10.1016/j.enconman.2017.04.079
- Marwaha, A., Dhir, A., Mahla, S. K., & Mohapatra, S. K. (2018). An overview of solid base heterogeneous catalysts for biodiesel production. *Catalysis Reviews Science and Engineering*, 60(4), 594–628. https://doi.org/10.1080/01614940.2018.1494782
- Mazaheri, H., Ong, H. C., Amini, Z., Masjuki, H. H., Mofijur, M., Su, C. H., Badruddin, I. A., & Yunus Khan, T. M. (2021). An overview of biodiesel production via calcium oxide based catalysts: Current state and perspective. *Energies*, 14(13). MDPI AG. https://doi.org/10.3390/en14133950
- Mengistu, N. G., Mekonen, M. W., Ayalew, Y. G., Demisie, L. F., & Nega, T. (2024). Experimental investigation on diesel engine performance and emission characteristics using waste cooking oil blended with diesel as biodiesel fuel. *Discover Energy*, 4(1), 26. https://doi.org/10.1007/s43937-024-00051-7
- Mora, J. M. R., Lacson, C. F. Z., Choi, A. E. S., Chung, T.-W., Retumban, J. D., Abarca, R. R., Grisdanurak, N., & de Luna, M. D. G. (2024). Biodiesel production from soybean oil via LiOH-pumice catalytic transesterification and BBD-RSM optimization. *Energy Reports*, 11(February), 4032–4043. https://doi.org/10.1016/j.egyr.2024.03.050
- Nguyen, V. G., Pham, M. T., Le, N. V. L., Le, H. C., Truong, T. H., & Cao, D. N. (2023). A comprehensive review on the use of biodiesel for diesel engines. *International Journal of Renewable Energy Development*, 12(4), 720–740. https://doi.org/10.14710/ijred.2023.54612
- Nisar, J., Razaq, R., Farooq, M., Iqbal, M., Khan, R. A., Sayed, M., Shah, A., & Rahman, I. ur. (2017). Enhanced biodiesel production from Jatropha oil using calcined waste animal bones as catalyst. Renewable Energy, 101, 111–119. https://doi.org/10.1016/j.renene.2016.08.048
- Novita, L., Safni, Emriadi, de Freitas, F. A., Fauzia, S., & Zein, R. (2024). Enhanced conversion of used palm cooking oil to biodiesel by a green and recyclable palm kernel shell ash-derived catalyst: Process optimization by response surface methodology. Case Studies in Chemical and Environmental Engineering, 9. https://doi.org/10.1016/j.cscee.2024.100678
- Olutoye, M. A., Wong, S. W., Chin, L. H., Amani, H., Asif, M., & Hameed, B. H. (2016). Synthesis of fatty acid methyl esters via the transesterification of waste cooking oil by methanol with a barium-modified montmorillonite K10 catalyst. *Renewable Energy*, 86, 392–398. https://doi.org/10.1016/j.renene.2015.08.016
- Pansakdanon, C., Seejandee, P., Kosawatthanakun, S., Deekamwong, K., Prayoonpokarach, S., & Wittayakun, J. (2025). Influence of crystallinity of zeolite NaX as a support for potassium catalyst in transesterification of palm oil. *Journal of Physics and Chemistry of Solids*, 196. https://doi.org/10.1016/j.jpcs.2024.112389
- Pavlović, S. M., Marinković, D. M., Kostić, M. D., Janković-Častvan, I. M., Mojović, L. V., Stanković, M. V., & Veljković, V. B. (2020). A CaO/zeolite-based catalyst obtained from waste chicken eggshell and coal fly ash for biodiesel production. *Fuel*, 267(September 2019), 117171. https://doi.org/10.1016/j.fuel.2020.117171

- Qu, S., Chen, C., Guo, M., Lu, J., Yi, W., Ding, J., & Miao, Z. (2020). Synthesis of MgO/ZSM-5 catalyst and optimization of process parameters for clean production of biodiesel from Spirulina platensis. *Journal of Cleaner Production*, 276, 123382. https://doi.org/10.1016/j.jclepro.2020.123382
- Rabie, A. M., Shaban, M., Abukhadra, M. R., Hosny, R., Ahmed, S. A., & Negm, N. A. (2019). Diatomite supported by CaO/MgO nanocomposite as heterogeneous catalyst for biodiesel production from waste cooking oil. *Journal of Molecular Liquids*, 279, 224–231. https://doi.org/10.1016/j.molliq.2019.01.096
- Saad, M., Siyo, B., & Alrakkad, H. (2023). Preparation and characterization of biodiesel from waste cooking oils using heterogeneous Catalyst(Cat.TS-7) based on natural zeolite. *Heliyon*, 9(6), e15836. https://doi.org/10.1016/j.heliyon.2023.e15836
- Sari, M. E. F., Suprapto, & Prasetyoko, D. (2018). Direct synthesis of sodalite from kaolin: The influence of alkalinity. *Indonesian Journal of Chemistry*, 18(4), 607–613. https://doi.org/10.22146/ijc.25191
- Shalaby, E. A., & Sh El-Gendy, N. (2012). Two steps alkaline transesterification of waste cooking oil and quality assessment of produced biodiesel. In *International Journal of Chemical and Biochemical Sciences*, 1. www.iscientific.org/Journal.html
- Shalihah, R., Widiarti, N., Yanuar, E., & Prasetyoko, D. (2020). Modified ZnO to Indonesia limestone as heterogeneous catalysts for biodiesel production from Reutealis trisperma oil. *Malaysian Journal of Fundamental and Applied Sciences*, 16(6), 649–653. https://doi.org/10.11113/mjfas.v16n6.1782
- Sun, H., Sun, K., Wang, F., Liu, Y., Ding, L., Xu, W., Sun, Y., & Jiang, J. (2021). Catalytic self-activation of Ca-doped coconut shell for insitu synthesis of hierarchical porous carbon supported CaO transesterification catalyst. *Fuel*, 285, 119192. https://doi.org/10.1016/j.fuel.2020.119192
- Supamathanon, N., Boonserm, K., Lisnund, S., Chanlek, N., Rungtaweevoranit, B., Khemthong, P., Wittayakun, J., & Osakoo, N. (2021). Development of CaO supported on modified geopolymer catalyst for transesterification of soybean oil to biodiesel. *Materials Today Communications*, 29, 102822. https://doi.org/10.1016/J.MTCOMM.2021.102822
- Szkudlarek, Ł., Chałupka-Śpiewak, K., Maniukiewicz, W., Nowosielska, M., Albińska, J., Szynkowska-Jóźwik, M. I., & Mierczyński, P. (2024). CaO catalysts supported on ZSM-5 zeolite for biodiesel production via transesterification of rapeseed oil. Applied Catalysis O: Open, 194, 206999. https://doi.org/10.1016/j.apcato.2024.206999
- Talebi, M., Larimi, A., Khorasheh, F., & Borhani, T. N. (2024). Biodiesel production using heterogeneous catalyst derived from natural calcite stone: Study of the effect of Mg–Zr doping and reaction conditions. Sustainable Chemistry and Pharmacy, 39. https://doi.org/10.1016/j.scp.2024.101559
- Tang, Z. E., Lim, S., Pang, Y. L., Ong, H. C., & Lee, K. T. (2018). Synthesis of biomass as heterogeneous catalyst for application in biodiesel production: State of the art and fundamental review. In Renewable and Sustainable Energy Reviews, 92, 235–253). https://doi.org/10.1016/j.rser.2018.04.056
- Ulfa, M., Masykur, A., Nofitasari, A. F., Sholeha, N. A., Suprapto, S., Bahruji, H., & Prasetyoko, D. (2022). Controlling the Size and Porosity of Sodalite Nanoparticles from Indonesian Kaolin for Pb2+ Removal. *Materials*, *15*(8). https://doi.org/10.3390/ma15082745
- Wahyuni, T., Prasetyoko, D., Suprapto, S., Qoniah, I., Bahruji, H., Dawam, A., Triwahyono, S., & Jalil, A. A. (2019). Direct synthesis of sodalite from Indonesian kaolin for adsorption of Pb2+ solution, kinetics, and isotherm approach. *Bulletin of Chemical Reaction Engineering & Catalysis*, 14(3), 502–512. https://doi.org/10.9767/bcrec.14.3.2939.502-512
- Weldeslase, M. G., Benti, N. E., Desta, M. A., & Mekonnen, Y. S. (2023).

  Maximizing biodiesel production from waste cooking oil with lime-based zinc-doped CaO using response surface methodology. *Scientific Reports*, 13(1), 1–14. https://doi.org/10.1038/s41598-023-30961-w
- Widiarti, N., Bahruji, H., Holilah, H., Ni'mah, Y. L., Ediati, R., Santoso, E., Jalil, A. A., Hamid, A., & Prasetyoko, D. (2021). Upgrading catalytic activity of NiO/CaO/MgO from natural limestone as catalysts for transesterification of coconut oil to biodiesel.

Biomass Conversion and Biorefinery. https://doi.org/10.1007/s13399-021-01373-5

Widayat, W.,Hantoro, S., Setyojati, P.W., , Shihab, D., Buchori, L., Hadiyanto, H., Nurushofa, F.A. (2024). Preparation CaO/MgO/Fe3O4 magnetite catalyst and catalytic test for biodiesel production. Results in Engineering, 22, art. no. 102202, https://doi.org/10.1016/j.rineng.2024.102202

Widiarti, N., Holilah, H., Bahruji, H., Nugraha, R. E., Suprapto, S., Ni'mah, Y. L., & Prasetyoko, D. (2024). Coprecipitation and hydrothermal synthesis of CaO from dolomite in the presence of Sapindus rarak extract for biodiesel production: catalysts

characterization and optimization. RSC Advances, 14(32), 23332–23340. https://doi.org/10.1039/d4ra03489a

Yang, J., Caldwell, C., Corscadden, K., He, Q. S., & Li, J. (2016). An evaluation of biodiesel production from Camelina sativa grown in Nova Scotia. *Industrial Crops and Products*, 81, 162–168. https://doi.org/10.1016/j.indcrop.2015.11.073

Yusuff, A. S., Gbadamosi, A. O., & Atray, N. (2022). Development of a zeolite supported CaO derived from chicken eggshell as active base catalyst for used cooking oil biodiesel production. Renewable Energy, 197, 1151–1162. https://doi.org/10.1016/j.renene.2022.08.032



© 2025. The Author(s). This article is an open access article distributed under the terms and conditions of the Creative Commons Attribution-ShareAlike 4.0 (CC BY-SA) International License (http://creativecommons.org/licenses/by-sa/4.0/)